ACS OMEGA

http://pubs.acs.org/journal/acsodf

Article

Structural Characteristics and Electrochemical Performance of N,P-Codoped Porous Carbon as a Lithium-Ion Battery Anode Electrode

Yun Liu,* Haihua Yang, Hongyu Zheng, Mengqiu Jia,* and Ao Huang

Cite This: *ACS Omega* 2022, 7, 34109−34116

Read Online

ACCESS | Metrics & More | Article Recommendations | Supporting Information

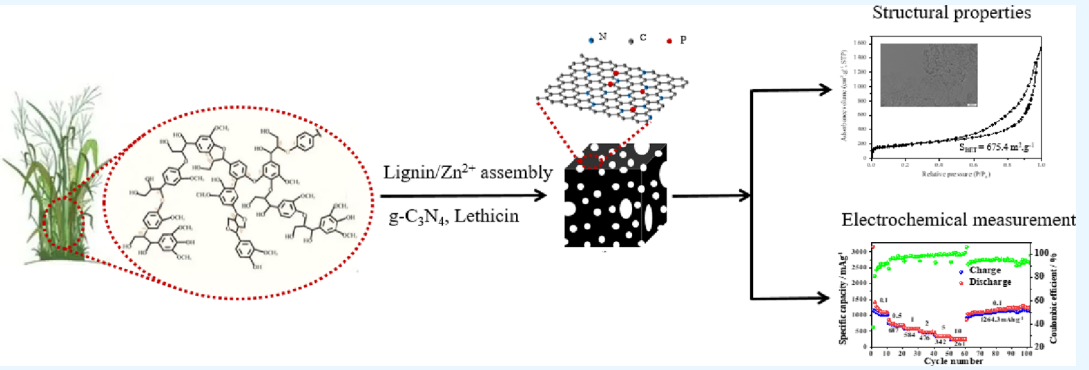

ABSTRACT: Biomass-derived heteroatom-doped carbons have been considered to be excellent lithium ion battery (LIB) anode materials. Herein, ultrathin g-C_3N_4 nanosheets anchored on N,P-codoped biomass-derived carbon (N,P@C) were successfully fabricated by carbonization in an argon atmosphere. The structural characteristics of the resultant N,P@C were elucidated by SEM, TEM, FTIR, XRD, XPS, Raman, and BET surface area measurements. The results show that N,P@C has a high specific surface area (S_{BET} = 675.4 cm^3/g), a mesoporous-dominant pore (average pore size of 6.898 nm), and a high level of defects (I_D/I_G = 1.02). The hierarchical porous structural properties are responsible for the efficient electrochemical performance of N,P@C as an anode material, which exhibits an outstanding reversible specific capacity of 1264.3 mAh/g at 100 mA/g, an elegant rate capability of 261 mAh/g at 10 A, and a satisfactory cycling stability of 1463.8 mAh/g at 1 A after 500 cycles. Because of the special structure and synergistic contributions from N and P heteroatoms, the resultant N,P@C endows LIBs with electrochemical performance superior to those of most of carbon-based anode materials derived from biomass in the literature. The findings in this present work pave a novel avenue toward lignin volarization to produce anode material for use in high-performance LIBs.

1. INTRODUCTION

Lithium ions batteries (LIBs) have garnered a large amount of attention from the public due to their prominent features of eminent power density, good cycle life, decreased pollution, and no memory effects.[1] Commercial LIBs are very suitable for use in various portable electronic devices and hybrid electric vehicles.[2] Recently, to bridge the gaps in energy capacity and reliable operation using graphite as a LIB anode, biomass-derived porous carbonaceous materials have been used as alternative anode electrodes for LIBs, including carbon nanotubes,[3] carbon nanofibers,[4] carbon nanobeads,[5] hollow carbon nanospheres,[6] graphene,[7] graphitic carbon,[8] hierarchical porous carbon,[9] and their hybrids.[10] However, more attention should be paid to improving the electrochemical performance of these biomass-derived carbonaceous anode electrodes.

Modifying carbonaceous anode electrodes by incorporating heteroatoms such as N, P, S, O, B, Sn, and Ge may imporove the electrochemical characteristics of anode electrode, since incorporating heteroatoms in the carbon skeleton can provide more active sites and increase the ion-storage capacity compared to that of pristine carbon.[11−13] For instance, N,O-codoped hierarchical porous carbon derived from biomass could enhance the wettability between the electrolyte and the electrode to deliver an eminent reversible capacity and an excellent cycling stability in LIBs.[11] N,P-Codoping could result in increased active site exposure for better electrochemical performance than that of sole-atom-doped carbon.[14,15] As anodes for LIBs, vesicle-structured Sn4P3@P/N dual-doped carbon nanocomposites (Sn4P3@PNC) exhibited good rate capabilities and satisfactory cycling stabilities, which were ascribed to the intimate contact of Sn_4P_3 with PNC and the

Received: May 31, 2022
Accepted: September 2, 2022
Published: September 13, 2022

© 2022 The Authors. Published by American Chemical Society

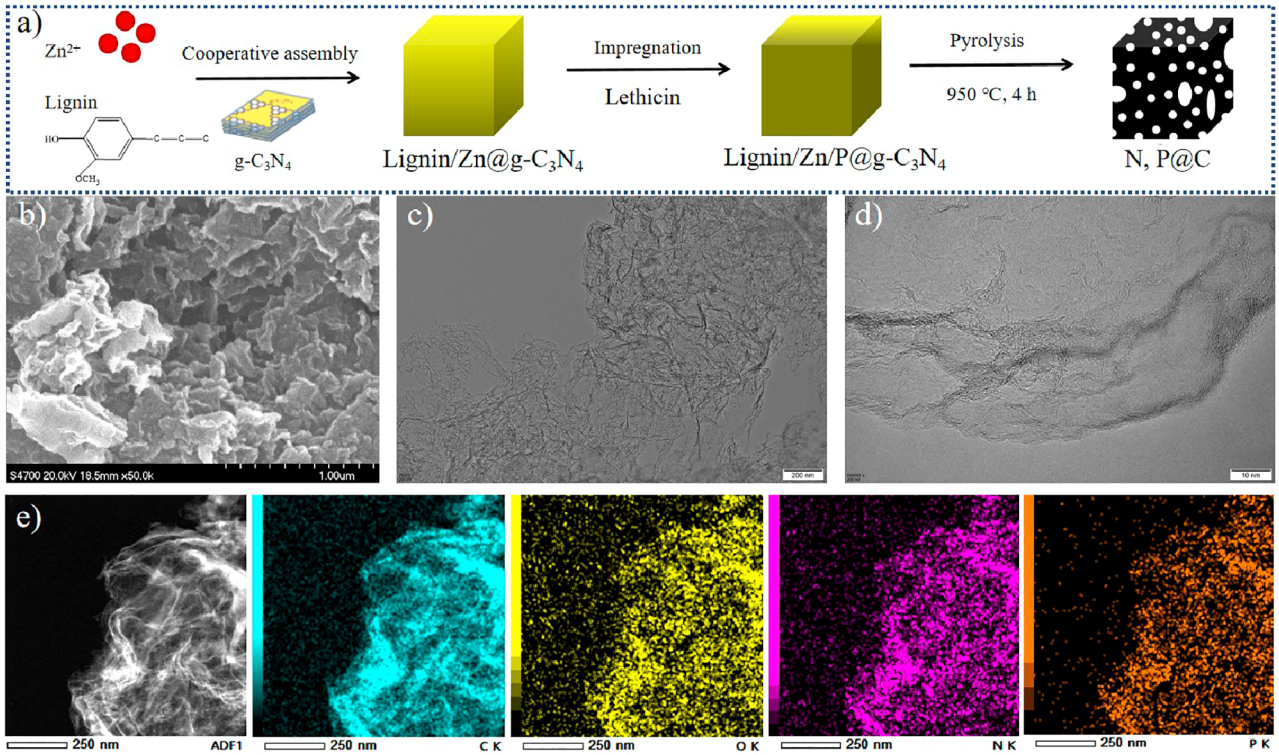

Figure 1. Overview of the synthesis procedure and morphology of N,P@C, which was imaged by SEM and TEM methods. (a) Synthesis scheme of N,P@C. (b) SEM image, (c) TEM image, (d) high-resolution transmission electron microscopy (HR-TEM) image, (e) and high-angle annular dark-field scanning transmission electron microscopy (HAADF-STEM) elemental mapping of N,P@C.

unique vesicle structure.[16] G,P-Codoped porous carbon nanoparticles (GPBN/C) were used as LIB anode materials with efficient electrochemical performance.[17] The higher the specific surface area and the pore volume of carbon materials, the higher the exposure of active sites and the energy density of batteries.[18] Therefore, adjusting the microstructure of the biomass-derived carbonaceous anode materials through heteroatom incorporation is of great importance to attain high electrochemical performance in LIBs systems.

Lignin, the largest aromatic biopolymer in nature, is a characteristic component of secondary walls of biomass, with a content of 15−30 wt %.[19] With the development of biomass biorefinery, the productivity of lignin has sharply increased in the last two decades. Lignin can be upgraded into biofuels, biochemicals, and biomaterials to facilitate the economic conversion of biomass toward a fossil-free society.[20] However, little information on lignin-derived porous carbon doped with heteroatoms as LIBs anode materials is avilable in the literature. A graphitic carbon ($g\text{-}C_3N_4$) nanosheet was always synthesized via a polycondensation reaction by annealing dicyandiamide, melamine, and urea at 550 °C in air for 4 h.[21,22] Researchers have demonstrated that $g\text{-}C_3N_4$ is a good interface enabler for depressing the formation of the dendritic lithium for solid-state lithium-metal batteries.[22−24] Additionally, $g\text{-}C_3N_4$ can also serve as a photocatalyst,[25] and $g\text{-}C_3N_4$-supported single-atom catalysts have been used for energy storage.[26] However, little information has been available on the use of an active carbon material with $g\text{-}C_3N_4$ as a soft template for LIB anodes so far.

In the present study, a simple carbonization approach is proposed to fabricate N,P-codoped lignin-derived hierarchical porous carbon (N,P@C) using $ZnCl_2$ as a pore-forming agent and $g\text{-}C_3N_4$ as a soft template for use as efficient anode material in LIBs. The structure of the as-obtained N,P@C was comprehensively elucidated by Fourier transform infrared spectroscopy (FT-IR), X-ray diffraction (XRD), scanning electron microscopy (SEM), Raman spectroscopy (Raman), transmission electron microscopy (TEM), X-ray photoelectron spectroscopy (XPS), and N_2 adsorption−desorption isotherm curves for Brunauer−Emmet−Teller (BET) surface area measurements. As counterparts, lignin-derived carbon (C) without a heteroatom dopant and N-doped lignin-derived carbon (N@C) and P-doped lignin-derived carbon (P@C) with a sole heteroatom dopant were also synthesized following a procedure similar to that for the synthesis of N,P@C . Serving as the anode electrode for LIBs, the as-obtained N,P@C exhibited a higher reversible specific capacity, a better rate capability, and a more satisfactory cycling stability than other carbonaceous counterparts derived from biomass.

2. MATERIALS AND METHODS

2.1. Materials. Ligin (lot no. 04414PEV, CAS 8068-05-1) and urea (A.R) were both available from Sigma Co. Ltd. (Shanghai, China). Polyvinylidene fluoride (PVDF), polyvinylpyrrolidone (PVP), and *N*-methyl pyrrolidone (NMP) were purchased from Beijing Chemical Factory (Beijing, China). Analytic-grade zinc chloride ($ZnCl_2$) and *N*,*N*-dimethylformamide (DMF) were purchased from Sinopharm Chemical Reagent Co. Ltd. (Shanghai, China). Lecithin (the content of elemental P was 2.7%) was gifted from Hebei Meiyesiwei Biological Technology Co. Ltd. (Hebei Province, China).

2.2. Fabrication of the N,P@C Material. The synthesis scheme for N,P-codoped lignin-derived carbon (N,P@C) is

https://doi.org/10.1021/acsomega.2c03400
ACS Omega 2022, 7, 34109−34116

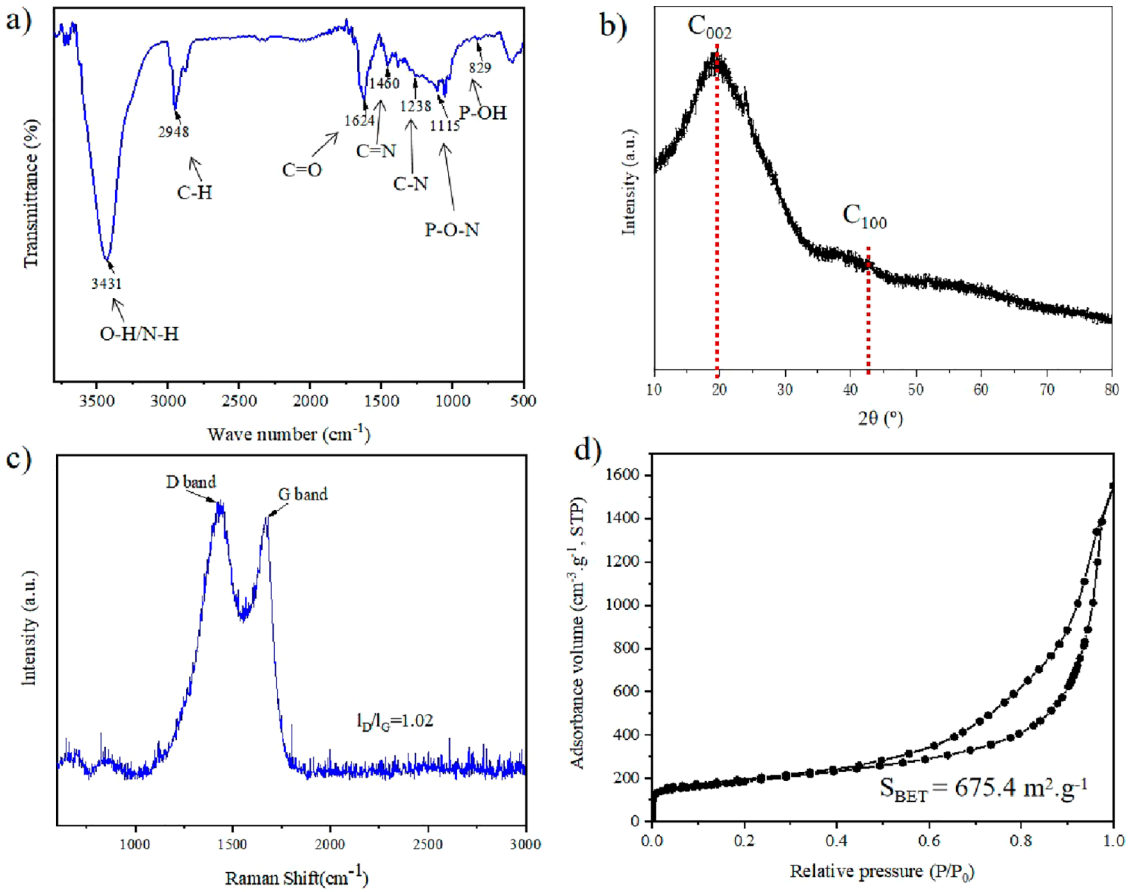

Figure 2. Structural properties of N,P@C as detected by FT-IR, XRD, Raman, and BET techniques. (a) FT-IR spectrum, (b) XRD pattern, (c) Raman spectrum, and (d) BET isothermal curve of N,P@C.

shown in Figure 1a. First, 10.5 g of g-C_3N_4 as the N source and a soft template was uniformly dispersed in 300 mL of deionized water, then 3.5 g of lignin and 14 mmol Zn^{2+} were dissolved in the water.[20,21] The mixture was stirred at a rotating speed of 800 rpm for 2 h and then aged at 25 °C for 12 h. Afterward, the mixture was centrifuged, and the residual solid was dried at 80 °C for 5 h to yield the g-C_3N_4 templated coated with lignin/Zn^{2+} coordination (lignin/Zn@g-C_3N_4). Subsequently, 100 mg of lecithin (the content of elemental P was 2.7%) was dissolved in 20 mL of ethanol under ultrasonic conditions for 30 min. Then, 3 g of lignin/Zn@g-C_3N_4 was dispersed in this solution, and the mixture was stirred at 800 rpm for 48 h. After being kept still overnight, the mixture was centrifuged at 5500 rpm for 15 min, and the residue solid was dried at 50 °C to yield the lignin/Zn/P@g-C_3N_4 composite.

Furthermore, 3 g of the lignin/Zn/P@g-C_3N_4 composite as a precursor was uniformly placed in a porcelain boat. The precursor in boat was annealed at a temperature program in a tube furnace with flowing argon gas. The temperature program was as follows: the temperature was increased from 25 to 550 °C with the heating rate of 25 °C/min and kept at 550 °C for 2 h, then increased to 950 °C with the heating rate of 10 °C/min and kept h at 950 °C for 4, and finally naturally cooled to 30 °C. The resultant solid was washed using DMF as the solvent for 36 h, then washed with deionized water to remove impurities. The treated solid was dried at 80 °C under vacuum conditions to obtain N,P-codoped lignin-derived carbon (N,P@C) sample.

As counterparts, lignin-derived carbon (C) without a heteroatom dopant and N-doped lignin-derived carbon (N@C) and P-doped lignin-derived carbon (P@C) with a sole heteroatom dopant were synthesized using a procedure similar to the aforementioned N,P@C synthesis.

2.3. Structural Characteristics of the N,P@C Material. The morphology images of N,P@C were recorded using a JEOLJSM-7500F SEM (Japan) and a JEM-2100F TEM (Japan). The crystalline phase of N,P@C was measured by XRD (Germany). The defect degree of N,P@C was determined by Raman spectroscopy. The linkage bond of N,P@C was confirmed by Fourier transform infrared spectroscopy (FT-IR); spectra were recorded from 500 to 4000 cm^{-1} at a resolution of 2 cm^{-1}. The specific surface areas and pore sizes of N,P@C were determined by nitrogen adsorption−desorption isotherm curves. The element compositions and species of N,P@C were analyzed by XPS.

2.4. Electrochemical Measurements. Electrochemical experiments for carbon materials include the preparation of a carbon-based working electrode and electrochemical activity measurements.[1,2] To prepare a carbon-based working electrode, a total weight of 18 mg of carbon material (14.4 mg, 80%), acetylene black (1.8 mg, 10%), and PVDF (1.8 mg, 10%) were evenly stirred and ground for 5 min. Afterward, the appropriate NMP was put into the mixture to form a diluted slurry. To prepare an anode plate, the slurry was blade-coated on the copper foil and then dried at 120 °C in a vacuum-drying oven for 12 h. The dried anode plate was then pressed into a wafer with a 1 cm diameter, which could be used as working

https://doi.org/10.1021/acsomega.2c03400
ACS Omega 2022, 7, 34109−34116

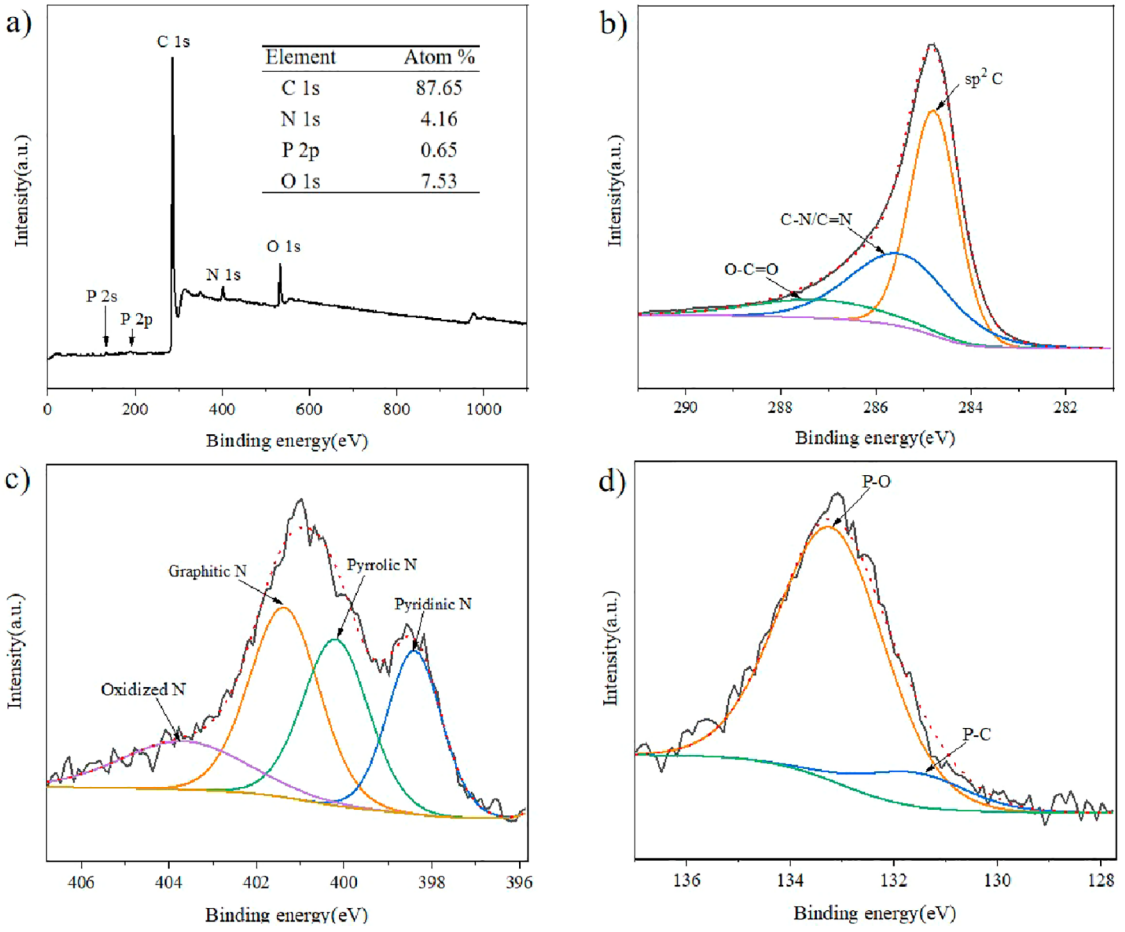

Figure 3. Elemental compositions and species of N,P@C measured by XPS. (a) XPS survey spectrum, (b) high-resolution XPS C 1s spectrum, (c) high-resolution XPS N 1s spectrum, and (d) high-resolution XPS P_{2p} spectrum of N,P@C.

electrode. Subsequently, CR2025 coin-type cells were prepared with the working electrode in an argon-filled glovebox in which the moisture and oxygen pressures were both less than 1.0 ppm. The reference electrode was lithium foil, and the electrolyte was 1.0 M $LiPF_6$ in a mixture of 50% ethylene carbonate (EC) and 50% diethyl carbonate (DEC). The electrochemical activity of the carbon-based working electrode was measured as follows: Cyclic voltammetry (CV) was conducted on a CS350 electrochemical workstation from 0 to 3.0 V with a 5 mV amplitude at a scan rate of 0.05 mV/s. The galvanostatic charge−discharge curves were recorded at 100 mA/g on a CT3008 battery test system in a voltage windows of 0.1−3.0 V. The rate capacity was tested at different current densities of 0.1, 0.5, 1, 2, 5, and 10 A for 10 cycles. The cycling performance and its corresponding Coulombic efficiency (CE) were both analyzed at 0.5 and 1 A/g for 500 cycles and at 5 A/g for 1000 cycles.

3. RESULTS AND DISCUSSION

The schematic for the fabrication of N,P@C and its morphology as imaged by SEM and TEM are shown in Figure 1. As shown in Figure 1a, a lignin/Zn^{2+} supermolecular composite was formed via the covalent coordination assembly of lignin and Zn^{2+} in an aqueous system at mild temperature, which was detailed in our previous work.[19] The lignin/Zn^{2+} supermolecular composite was coated on a g-C_3N_4 nanosheet to achieve lignin/Zn@g-C_3N_4 complexes. Afterward, P was impregnated into the lignin/Zn@g-C_3N_4 framework in an ethanol solution using lethicin as the P source. Subsequently, the precursor lignin/Zn/P@g-C_3N_4 was annealed in a tube furnace in an argon atmosphere to yield the N,P@C sample. At 950 °C the occurrence of phenomena of Zn^{2+} evaporation, g-C_3N_4 decomposition, and lignin graphitization could result in the hierarchical porous structure with defect carbon of N,P@C due to the rearrangement of carbon atoms.[21]

As shown by the SEM image in Figure 1b, the morphology of the resultant N,P@C is a stacked wrinkle nanosheet, similar to N@C (Figure S1) produced using ultrathin g-C_3N_4 as a soft template. In contrast, the morphologies of the lignin/Zn^{2+} assembly, C, and P@C imaged by SEM are smooth without the g-C_3N_4 template (Figure S1). The TEM image of N,P@C in Figure 1c shows the layered silk-like structure of the sample, indicating the ultrathin feature of the nanosheets. The HR-TEM image in Figure 1d confirms the presence of a large quantity of pores in the N,P@C material with a degree of low graphitization. It was demonstrated that these tiny pores could offer reservoirs for lithium ion storage, which improved the LIB capacity significantly.[1] HAADF-STEM elemental mapping (Figure 1e) points out that elements N and P are uniformly distributed on the surface of N,P@C. The codoping of N and P into the final porous carbonaceous material is further confirmed by the FT-IR and XPS spectra in Figure 2a and Figure 3, respectively.

https://doi.org/10.1021/acsomega.2c03400
ACS Omega 2022, 7, 34109−34116

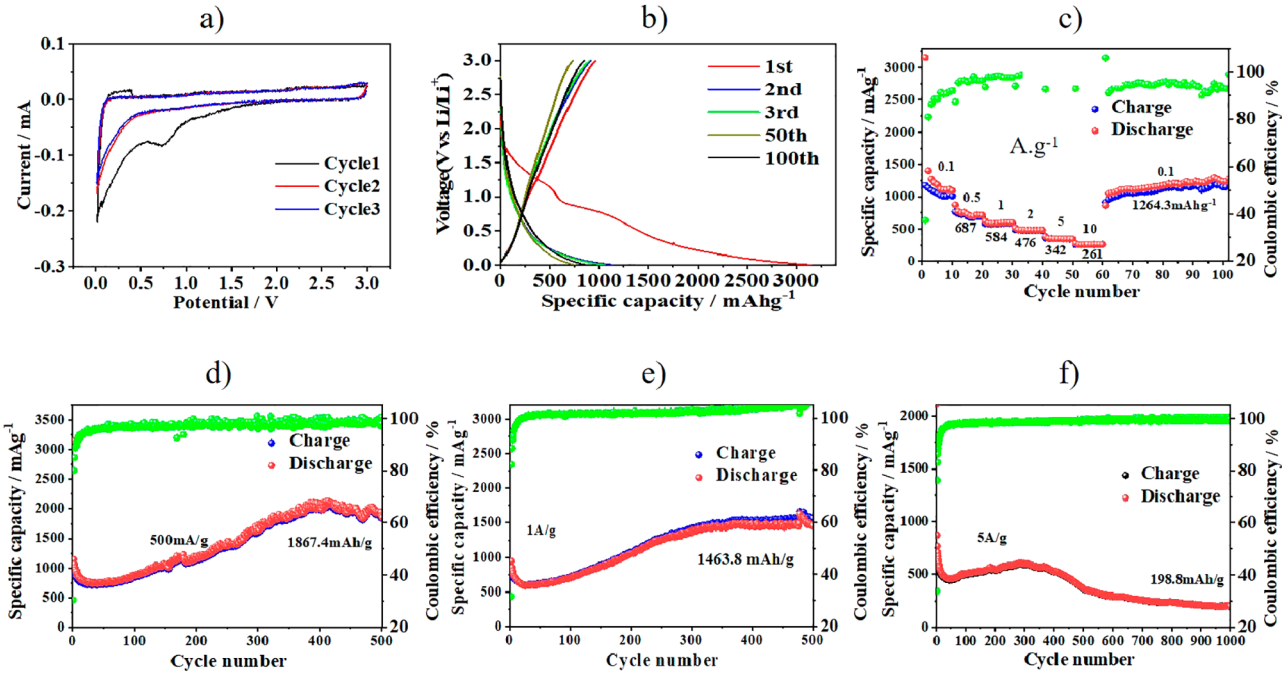

Figure 4. Electrochemical performances of the N,P@C anode material. (a) Cyclic voltammetry curves of three cycles in voltage windows from 0.1 to 3.0 V at 100 mA/g. (b) Galvanostatic charge−discharge curves at 100 mA/g. (c) Rate capability at different current densities of 01, 0.5, 1, 2, 5, and 10 A. (d) Cycling performance and Coulombic efficiency at 500 mA/g. (e) Cycling performance and Coulombic efficiency at 1 A/g. (f) Cycling performance and Coulombic efficiency at 5 A/g.

Furthermore, XRD, Raman, FT-IR, and BET measurements were conducted to shed light on the detailed structural information on N,P@C. The results are shown in Figure 2.

The FT-IR spectrum in Figure 2a reveals bands at 1460 and 1238 cm^{-1} that are assigned to the C−N linkage bond and bands at 1115 and 829 cm^{-1} that are ascribed to the P−O linkage bond.[14] It suggests that heteroatoms N and P are codoped into the N,P@C material. This result agrees well with the HAADF-STEM image in Figure 1e. The XRD pattern in Figure 2b displays a relatively strong and broad graphitic carbon (002) peak at about 20° and a weak and narrow carbon (100) peak at 42°, revealing the formation of graphitic carbon during the pyrolysis treatment. Similar XRD patterns were also found in C, N@C, and P@C materials (Figure S2). This means that pyrolysis treatment of carbon is prone to causing graphitization.[1,2,19−21,27] Studies have revealed that the graphitic carbon framework is beneficial for Li^+ ion intercalation and diffusion.[28,29]

Raman spectroscopy was further conducted to measure the graphitization degree of N,P@C. As shown in Figure 2c, two distinct signal peaks are present at 1342 (D band, ascribed to disorder and defective graphitic structure) and 1599 cm^{-1} (G band, assigned to ordered graphitic carbon), and the I_D/I_G intensity ration is 1.02. This indicates that N,P@C tends to be a disordered amorphous or defective carbon framework due to heteroatom doping and Zn^{2+} evaporation.[11,27,30] The graphitization degree of N,P@C (I_D/I_G = 1.02) is higher than that of its counterparts (Figure S3) C (I_D/I_G = 1.15), N@C (I_D/I_G = 1.04), and P@C (I_D/I_G = 1.11). The improved graphitization structure of N,P@C can expose more active sites for lithium ion intercalation and transportation.[31,32]

The BET specific surface area (S_{BET}) and pore structure of the carbon material are two important indicators of lithium ion intercalation and deinsertion.[28] The N_2 adsorption−desorption isotherm curve of N,P@C in Figure 2d exhibits the characteristic type IV isotherm with a clear H3 hysteresis loop, which indicates that N,P@C has hierarchical porous features of micro-, meso-, and macropores.[33] Many researchers have demonstrated that macropores can provide transportation channels for lithium ion diffusion, micropores can act as reservoirs to improve the capacity of lithium ion storage, and mesopores offer highways for lithium ion transportation.[9,11,33−36] The values for S_{BET}, the average pore size, and the pore volume of N,P@C were calculated to 675.4 m^2/g, 6.898 nm, and 2.383 cm^3/g, respectively. In comparison with most of the biomass-derived anode materials in the literature, N,P@C shows higher S_{BET} value, which is associated with the synthesis procedure of the carbon material.[1,32,37] Both the high S_{BET} value and the hierarchical pore structure benefit the efficient electrochemical performance of lithium ion battery by exposing more active sites and facilitating lithium ion diffusion.[37,38]

To further explore the elemental compositions and species of N,P@C, XPS survey spectra were recorded, as shown in Figure 3. The existence of C, N, and P peaks in the XPS survey spectrum (Figure 3a) further confirms the multiheteroatom codoping of the final carbon skeleton with N and P elements. This phenomenon is also demonstrated by the HAADF-STEM (Figure 1e) and FTIR (Figure 2a) results. The presence of the O peak in Figure 3a reveals oxygen residue in the final carbon material from the lignin starting material (the content of elemental O ranges from 35 to 53 at %). The element composition of N,P@C are mainly consisted of carbon (87.65 at %), nitrogen (4,16 at %), phosphorus (0.65 at %), and oxygen (7.53 at %) (Figure 3a). As can be seen from the high-resolution XPS C 1s spectrum in Figure 3, the weak O—C═O peak at 287.9 eV is deconvoluted, suggesting that the source of the oxygen element was probably the oxygenated groups on

https://doi.org/10.1021/acsomega.2c03400
ACS Omega 2022, 7, 34109−34116

lignin.[14] Two strong peaks are deconvoluted, namely, the C═C peak at 284.6 eV (ascribed to sp^2 graphitic carbon) and the C—N/C═N peak at 285.6 eV (ascribed to C-bonded carbon), indicating the successful N-doping in the final carbonized sample.[39] As seen from the high-resolution XPS N 1s spectrum in Figure 3c, four peaks are deconvoluted: that for oxidized N at 403.8 eV, that for graphitic N at 401.6 eV, that for pyrrolic N at 400.2 eV, and that for pyridinic N at 398.5 eV.[14] In the high-resolution XPS P_{2p} spectrum shown from Figure 3d, two peaks are fitted: that for the P−C bond at approximately 131.6 eV and that for the P−O bond at approximately 133.2 eV.[14] Therefore, the XPS survey spectra of N,P@C demonstrate the desired elemental composition (C, N, P, and O) without any other impurity contamination. A heteroatom dopant (like N, O, and P) can enhance the electrochemical performance by enhancing the reactive activity and offering lots of ion storage sites.[7,11,40]

After elucidating the structural properties, experiments on the electrochemical performance of N,P@C were further carried out, and the results are shown in Figure 4.

The lithium ion storage behavior of N,P@C can be understood from the CV measurement. As shown in from Figures 4a and S4, the CV curves of the as-obtained carbon materials, namely, N,P@C, C, N@C, and P@C, are similar in shape and reduction potential except for the reversibility of the first cycle. The broad irreversible negative peak at about 0.75 V of the first cycle is characteristic of CV curves of biomass-derived carbon as anode material. The probably reasonable explanation is the decomposition of the electrolyte and the formation of a solid electrolyte interface (SEI) film.[2,4,5,41,42] In the second and third cycles, this wide reduction peak disappears, and the CV curves overlap. The galvanostatic charge−discharge curve of N,P@C in Figure 4b shows that the initial charge specific capacity is 1106 mAh/g and the corresponding initial CE is approximately 37%, slightly higher than those of C (31%), N@C (34%) and P@C (32%) (Figure S5). It is universally acknowledged that a low CE is a big challenge in the practical application of biomass-derived carbons as LIBs anode materials.[1,2,41−45]

Appealingly, the N,P@C anode retains its high Li^+ ion storage and excellent rate capability (Figure 4c). As shown in Figure 4c, the reversible capacities at 0.1, 0.5, 1, 2, 5, and 10 A/g for 10 cycles were calculated to be approximately 1260, 687, 584, 476, 342, and 261 mAh/g, respectively. Even at an extremely high current density of 10 A/g, the reversible capacity remained 261 mAh g^{-1}, approximately 70% the theoretical capacity of graphite (372 mAh/g). It should be noticed that the discharge capacity of N,P@C can recover 1264.3 mAh/g when the current density is returned to 0.1 A/g. As an example, the rate capability curves of the N@C counterpart are shown in Figure S6a; its discharge capacity is greatly inferior to that of N,P@C when the current density is returned to 0.1 A/g (Figure S6b). The reasonable explanation is ascribed to the synergistic contributions of heteroatom doping.[4,7,11−13,32,39,40] These data indicate that the N,P@C anode shows a good rate capability and excellent reversibility.

Furthermore, the long cycling performace of N,P@C was tested to evaluate its durability at 0.5 and 1 A after 500 cycles and at 5 A after 1000 cycles. As shown in Figure 4d, the reversible specific capacity of N,P@C is 1867.4 mAh/g at 0.5 A after 500 cycles, while the reversible specific capacities of C, N@C, and P@C are only 241.8, 547, and 230 mAh/g, respectively (Figure S7). The highly efficient performance of the N,P@C anode is ascribed to the combined effects of both the mesoporous-dominant hierarchical structure with a large S_{BET} and the synergistic contribution of heteroatom doping.[7,10−14,27,28,31,32] As shown by the TEM images in Figure S8a and b, the morphology of the used N,P@C anode remains intact at a relative low current density of 0.5 A after 500 cycles, confirming the satisfactory structural stability of the N,P@C material. However, the thermostability of the used N,P@C material is higher after 500 cycles than that of the pristine material (Figure S8c). This can probably be ascribed to some Li^+ ion adsorption on the interlayer and surface of N,P@C after cycling. When the current density was increased to 1 A/g (Figure 4e), N,P@C showed a stable capacity of 1463.8 mAh/g after 500 cycles, a durability than that of N@C. When the current density was further enhanced to 5 A/g, the reversible specific capacity of N,P@C was about 625.8 mAh/g after 500 cycles and 198 mAh/g after 1000 cycles (Figure 4f). The decrease in capacity during cycling mainly arises from the structural destruction caused by large quantities of defects at a high current density of 5 A/g. As an example, the cycling performance and the corresponding CE of N@C were examined at 1, 2, and 5 A/g. It can be observed in Figures S9a and c that N@C has a much lower stable capacity at 1 (471 mAh/g after 500 cycles) and 5 A/g (115.5 mAh/g after 1000 cycles).

To better highlight the electrochemical performance of N,P@C, an impedance test was conducted in lithium batteries, and the result is shown in Figure 5.

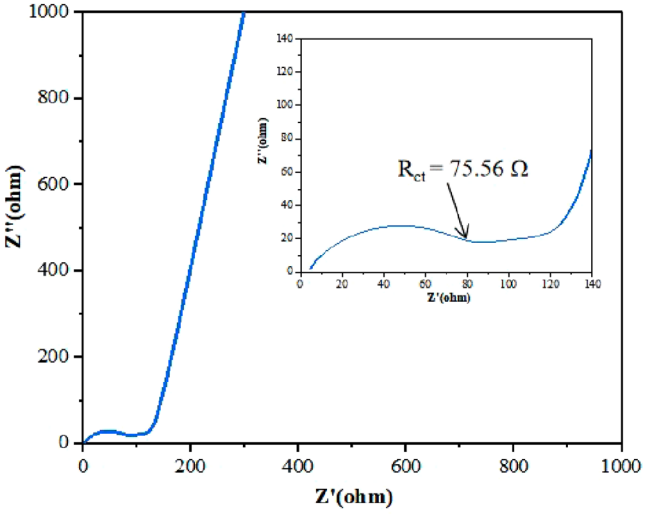

Figure 5. Electrochemical impedance spectra of N,P@C in lithium batteries.

As shown in Figure 5, the Ohmic resistance at the high-frequency semicircle expresses the resistance of the electrolyte or the contact resistance,[46] while the Warburg impedance at the lower-frequency inclined line at approximately 45° is associated with the diffusion of Li^+ ions in the carbon anode electrode.[47] As can be observed from the Nyquist plot in the inset of the figure, the charge transfers resistance (R_{ct}) of the N,P@C anode electrode was found to be 75.56 Ω, significantly lower than those of biomass-derived carbon from ramie fiber (R_{ct} = 239.7 Ω) and corncob (R_{ct} = 129.2 Ω).[48] This indicates that the electronic conductivity of the N,P@C electrode is satisfactory in a LIB system.

https://doi.org/10.1021/acsomega.2c03400
ACS Omega 2022, 7, 34109−34116

Based on is outstanding cycling performance and satisfactory reversibility, lignin-derived N,P@C shows potential for promising practical applications as an anode material in LIBs. Table S1 comprehensively compares the electrochemical performance of lignin-derived N,P@C and those of biomass-derived carbonaceous materials in LIBs. Obviously, the specific capability of N,P@C is much better than those of most biomass-derived carbonaceous anode materials in the literature (Table S1). Although a lot of research on biomass-derived carbonaceous anode materials has been reported, more efforts should be made to improve the specific capacity of batteries and the initial CE in the coming practical applications.

4. CONCLUSIONS

In summary, N,P@C was successfully fabricated by coating a lignin/Zn^+ composite on a g-C_3N_4 soft template, followed by an annealing procedure using lecithin as P source. The resultant N,P@C was characterized by SEM, TEM, FTIR, XRD, XPS, Raman spectroscopy, and BET surface area measurements. The combined effects of the hierarchical porous structure, the high S_{BET}, and the synergistic contribution of multiheteroatom dopants are responsible for the outstanding reversible capacity, excellent rate capability, and satisfactory cycling performance of N,P@C as an anode material in LIBs. Compared to previous research on electrochemical performance, the specific capacity N,P@C is superior those of most biomass-derived carbonaceous anode materials in earlier works. The findings not only reveal that N,P@C is a promising potential anode material in practical LIB applications but also paves a novel avenue for lignin valorization toward battery anode materials.

■ ASSOCIATED CONTENT

Supporting Information

The Supporting Information is available free of charge at https://pubs.acs.org/doi/10.1021/acsomega.2c03400.

SEM images, XRD patterns, Raman spectra, CV curves, galvanostatic charge−discharge curves, rate capability, cycling performance and its corresponding Coulombic efficiency, TEM images, TGA curves, and electrochemical performance comparison (PDF)

■ AUTHOR INFORMATION

Corresponding Authors

Yun Liu − *Beijing Key Laboratory of Bioprocess, College of Life Science and Technology, Beijing University of Chemical Technology, Beijing 100029, China;* orcid.org/0000-0002-7521-3831; Email: liuyun@mail.buct.edu.cn

Mengqiu Jia − *Beijing Key Laboratory of Bioprocess, College of Life Science and Technology, Beijing University of Chemical Technology, Beijing 100029, China; Beijing Key Laboratory of Electrochemical Process and Technology for Materials, Beijing University of Chemical Technology, Beijing 100029, China*; Phone: +86-010-64421335; Email: jiamengqiu@mail.buct.edu.cn; Fax: +86-010-64416428

Authors

Haihua Yang − *Beijing Key Laboratory of Bioprocess, College of Life Science and Technology, Beijing University of Chemical Technology, Beijing 100029, China*

Hongyu Zheng − *Beijing Key Laboratory of Electrochemical Process and Technology for Materials, Beijing University of Chemical Technology, Beijing 100029, China*

Ao Huang − *Beijing Key Laboratory of Bioprocess, College of Life Science and Technology, Beijing University of Chemical Technology, Beijing 100029, China*

Complete contact information is available at: https://pubs.acs.org/10.1021/acsomega.2c03400

Notes

The authors declare no competing financial interest.

■ ACKNOWLEDGMENTS

This study was funded by The National Key Research and Development Program of China (2021YFC2101304).

■ REFERENCES

(1) Yu, X.; Zhang, K.; Tian, N.; Qin, A.; Liao, L.; Du, R.; Wei, C. Biomass carbon derived from sisal fiber as anode material for lithium-ion batteries. *Mater. Lett.* **2015**, *142*, 193−196.

(2) Sankar, S.; Saravanan, S.; Ahmed, A. T. A.; Inamdar, A. I.; Im, H.; Lee, S.; Kim, D. Y. Spherical activated-carbon nanoparticles derived from biomass green tea wastes for anode material of lithium-ion battery. *Mater. Lett.* **2019**, *240*, 189−192.

(3) Li, T.; Wang, L.; Li, J. Carbon nanotube enables high-performance thiophene containing organic anodes for lithium ion batteries. *Electrochim. Acta* **2022**, *408*, 139947.

(4) Jiang, Q.; Ni, Y.; Zhang, Q.; Gao, J.; Wang, Z.; Yin, H.; Jing, Y.; Wang, J. Sustainable nitrogen self-doped carbon nanofibers from biomass chitin as anodes for high-performance lithium-ion batteries. *Energy Fuels.* **2022**, *36*, 4026−4033.

(5) Chang, J. C.; Tzeng, Y. F.; Chen, J. M.; Chiu, H. T.; Lee, C. Y. Carbon nanobeads as an anode material on high rate capability lithium ion batteries. *Electrochim. Acta* **2009**, *54*, 7066−7070.

(6) Zhao, F.; Li, X.; He, J.; Wang, K.; Huang, C. Preparation of hierarchical graphdiyne hollow nanospheres as anode for lithium-ion batteries. *Chem.Eng. J.* **2021**, *413*, 127486.

(7) Aghamohammadi, H.; Hassanzadeh, N.; Eslami-Farsani, R. A review study on the recent advances in developing the heteroatom-doped graphene and porous graphene as superior anode materials for Li-ion batteries. *Ceram. Int.* **2021**, *47*, 22269−22301.

(8) Liu, S.; Ren, Z.; Fakudze, S.; Shang, Q.; Chen, J.; Liu, C.; Han, J.; Tian, Z. Structural evolution of graphitic carbon derived from ionic liquids-dissolved cellulose and its application as lithium-ion battery anodes. *Langmuir.* **2022**, *38*, 320−331.

(9) Hwang, S. Y.; Lee, H. R.; Lee, Y. K.; Lee, G. B.; Lee, S.; Kim, H. J.; Joh, H. I. Stable fast-charging electrodes derived from hierarchical porous carbon for lithium-ion batteries. *Energy Res.* **2021**, *45*, 4718−4726.

(10) Tung, T. T.; Moussa, M.; Tripathi, K. M.; Kim, T.; Nine, M. J.; Nanjundan, A. K.; Dubal, D.; Losic, D. Coupling graphene microribbons with carbon nanofibers: New carbon hybrids for high-performing lithium and potassium-ion batteries. *Sustain. Mater. Technol.* **2022**, *32*, No. e00393.

(11) Fan, W.; Zhang, H.; Wang, H.; Zhao, X.; Sun, S.; Shi, J.; Huang, M.; Liu, W.; Zheng, Y.; Li, P. Dual-doped hierarchical porous carbon derived from biomass for advanced supercapacitors and lithium ion batteries. *RSC Adv.* **2019**, *9*, 32382−32394.

(12) Liu, B.; Sun, X.; Liao, Z.; Lu, X.; Zhang, L.; Hao, G. P. Nitrogen and boron doped carbon layer coated multiwall carbon nanotubes as high performance anode materials for lithium ion batteries. *Sci. Rep.* **2021**, *11*, 5633.

(13) Cheng, X.; Ran, F.; Huang, Y.; Zheng, R.; Yu, H.; Shu, J.; Xie, Y.; He, Y. B. Insight into the synergistic effect of N, S co-doping for carbon coating layer on niobium oxide anodes with ultra-long life. *Adv. Funct. Mater.* **2021**, *31*, 2100311.

(14) Zhang, J.; Qu, L.; Shi, G.; Liu, J.; Chen, J.; Dai, L. N,P-codoped carbon networks as efficient metal-free bifunctional catalysts for oxygen reduction and hydrogen evolution reactions. *Angew. Chem.* **2016**, *128*, 2270−2274.
(15) Zhao, J.; Wei, D.; Zhang, X.; Zhang, S.; Zhang, C.; Yang, X. Biomass-derived hierarchical N, P codoped porous 3D-carbon framework@TiO_2 hybrids as advanced anode for lithium ion batteries. *J. Colloid Interface Sci.* **2022**, *606*, 577−587.
(16) Xia, S.-X.; Yan, Y.-H.; Sun, H.; Yang, J.-H.; Zheng, S.-Y. Engineering unique vesicle structured tin phosphides@P/N codoped carbon anode for high-performance sodium/lithium-ion batteries. *Rare Met.* **2022**, *41*, 1496−1503.
(17) Yan, Y.; Ruan, J.; Xu, H.; Xu, Y.; Pang, Y.; Yang, J.; Zheng, S. Fast and stable batteries with high capacity enabled by germanium-phosphorus binary nanoparticles embedded in a porous carbon matrix via metallothermic reduction. *ACS Appl. Mater. Interfaces* **2020**, *12*, 21579−21585.
(18) Li, X.; Wang, X.; Sun, J. Recent progress in the carbon-based frameworks for high specific capacity anodes/cathode in lithium/sodium ion batteries. *New Carbon Mater.* **2021**, *36*, 106−116.
(19) Zhou, H.; Zhang, R.; Zhan, W.; Wang, L.; Guo, L.; Liu, Y. High biomass loadings of 40 wt.% for efficient fractionation to meet biorefinery in solvent aqueous system without adding adscititious catalyst. *Green Chem.* **2016**, *18*, 6108−6114.
(20) Liu, Y.; Xu, H.; Yu, H.; Yang, H.; Chen, T. Synthesis of lignin-derived nitrogen-doped carbon as a novel catalyst for 4-NP reduction evaluation. *Sci. Rep.* **2020**, *10*, 20075.
(21) Liu, Y.; Yang, H.; Chen, T. Nitrogen-doped lignin-derived carbon for catalytic reduction of hexavalent chromium via HCOOH mediated hydrogenation. *RSC Adv.* **2022**, *12*, 4550−4561.
(22) Huang, Y.; Chen, B.; Duan, J.; Yang, F.; Wang, T.; Wang, Z.; Yang, W.; Hu, C.; Luo, W.; Huang, Y. Graphitic Carbon Nitride (g-C_3N_4): An interface enabler for solid-state lithium metal Batteries. *Angew. Chem., Int. Ed.* **2020**, *59* (9), 3699−3704.
(23) Ye, S.; Wang, L.; Liu, F.; Shi, P.; Wang, H.; Wu, X.; Yu, Y. g-C_3N_4 Derivative artificial organic/inorganic composite solid electrolyte interphase layer for stable lithium metal anode. *Adv. Energy Mater.* **2020**, *10* (44), 2002647.
(24) Hu, J.; Tian, J.; Li, C. Nanostructured carbon nitride polymer-reinforced electrolyte to enable dendrite-suppressed lithium metal batteries. *ACS Appl. Mater. Interfaces* **2017**, *9*, 11615−11625.
(25) Li, Y.; Jin, R.; Xing, Y.; Li, J.; Song, S.; Liu, X.; Li, M.; Jin, R. Macroscopic foam-like holey ultrathin g-C_3N_4 nanosheets for drastic improvement of visible-light photocatalytic activity. *Adv. Energy Mater.* **2016**, *6*, 1601273.
(26) Zhao, M.; Feng, J.; Yang, W.; Song, S.; Zhang, H. Recent advances in graphitic carbon nitride supported single atom catalysts for energy conversion. *ChemCatChem.* **2021**, *13*, 1250−1270.
(27) Zhou, H.; Hong, S.; Zhang, H.; Chen, Y.; Xu, H.; Wang, X.; Jiang, Z.; Chen, S.; Liu, Y. Toward biomass-based single-atom catalysts and plastics: Highly active single-atom Co on N-doped carbon for oxidative esterification of primary alcohols. *Appl. Catal., B* **2019**, *256*, 117767.
(28) Zhang, H.; Yang, Y.; Ren, D.; Wang, L.; He, X. Graphite as anode materials: Fundamental mechanism, recent progress and advances. *Energy Storage Mater.* **2021**, *36*, 147−170.
(29) Xu, C.; Ma, G.; Yang, W.; Che, S.; Li, Y.; Jia, Y.; Liu, H.; Chen, F.; Zhang, G.; Liu, H.; Wu, N.; Huang, G.; Li, Y. One-step reconstruction of acid treated spent graphite for high capacity and fast charging lithium-ion batteries. *Electrochim. Acta* **2022**, *415*, 140198.
(30) Wu, Z. S.; Ren, W.; Xu, L.; Li, F.; Cheng, H. M. Doped graphene sheets as anode materials with superhigh rate and large capacity for lithium ion batteries. *ACS Nano* **2011**, *5*, 5463−5471.
(31) Bhattacharjya, D.; Park, H. Y.; Kim, M. S.; Choi, H. S.; Inamdar, S. N.; Yu, J. S. Nitrogen-doped carbon nanoparticles by flame synthesis as anode material for rechargeable lithium-ion batteries. *Langmuir.* **2014**, *30*, 318−324.
(32) Ou, J.; Deng, H.; Zhang, H.; Wang, H. Nitrogen and phosphorus co-doped porous carbon prepared by direct carbonization method as potential anode material for Li-ion batteries. *Diam. Relat. Mater.* **2022**, *124*, 108931.
(33) Qiu, D.; Kang, C.; Li, M.; Wei, J.; Hou, Z.; Wang, F.; Yang, R. Biomass-derived mesopore-dominant hierarchical porous carbon enabling ultra-efficient lithium ion storage. *Carbon.* **2020**, *162*, 595−603.
(34) Dou, Y.; Liu, X.; Yu, K.; Wang, X.; Liu, W.; Liang, J.; Liang, C. Biomass porous carbon derived from jute fiber as anode materials for lithium-ion batteries. *Diam. Relat. Mater.* **2019**, *98*, 107514.
(35) Wang, K. X.; Li, X. H.; Chen, J. S. Surface and interface engineering of electrode materials for lithium-ion batteries. *Adv. Mater.* **2015**, *27*, 527−545.
(36) Tian, W.-Q.; Wu, X.-Y.; Wang, K.-X.; Jiang, Y.-M.; Wang, J.-F.; Chen, J.-S. Hierarchical porous carbon spheres as an anode material for lithium ion batteries. *RSC Adv.* **2013**, *3*, 10823−10827.
(37) Yuan, G.; Zhang, W.; Li, H.; Xie, Y.; Hu, H.; Xiao, Y.; Liang, Y.; Liu, Y.; Liu, W. R.; Zheng, M. Non-tubular-biomass-derived nitrogen-doped carbon microtubes for ultrahigh-area-capacity lithium-ion batteries. *J. Colloid Interface Sci.* **2020**, *580*, 638−644.
(38) Zhang, W.; Yin, J.; Lin, Z.; Lin, H.; Lu, H.; Wang, Y.; Huang, W. Facile preparation of 3D hierarchical porous carbon from lignin for the anode material in lithium ion battery with high rate performance. *Electrochim. Acta* **2015**, *176*, 1136−1142.
(39) Lin, D.; Hu, C.; Chen, H.; Qu, J.; Dai, L. Microporous N,P-codoped graphitic nanosheets as an efficient electrocatalyst for oxygen reduction in whole pH range for energy conversion and biosensing dissolved oxygen. *Chem. -Eur. J.* **2018**, *24*, 18487−18493.
(40) Bosubabu, D.; Sampathkumar, R.; Karkera, G.; Ramesha, K. Facile approach to prepare multiple heteroatom-doped carbon material from bagasse and its applications toward lithium-ion and lithium-sulfur batteries. *Energy Fuels* **2021**, *35*, 8286−8294.
(41) Qie, L.; Chen, W. M.; Wang, Z. H.; Shao, Q. G.; Li, X.; Yuan, L. X.; Hu, X. L.; Zhang, W. X.; Huang, Y. H. Nitrogen-doped porous carbon nanofiber webs as anodes for lithium ion batteries with a superhigh capacity and rate capability. *Adv. Mater.* **2012**, *24*, 2047−2050.
(42) Zheng, F.; Liu, D.; Xia, G.; Yang, Y.; Liu, T.; Wu, M.; Chen, Q. Biomass waste inspired nitrogen-doped porous carbon materials as high-performance anode for lithium-ion batteries. *J. Alloys Comp.* **2017**, *693*, 1197−1204.
(43) Xi, Y.; Yang, D.; Qiu, X.; Wang, H.; Huang, J.; Li, Q. Renewable lignin-based carbon with a remarkable electrochemical performance from potassium compound activation. *Ind. Crops prod.* **2018**, *124*, 747−754.
(44) Liu, Y.; Shi, M.; Yan, C.; Zhuo, Q.; Wu, H.; Wang, L.; Liu, H.; Guo, Z. Inspired cheese-like biomass-derived carbon with plentiful heteroatoms for high performance energy storage. *J. Mater. Sci.-Mater. Electron.* **2019**, *30*, 6583−6592.
(45) Tao, L.; Huang, Y.; Zheng, Y.; Yang, X.; Liu, C.; Di, M.; Larpkiattaworn, S.; Nimlos, M. R.; Zheng, Z. Porous carbon nanofiber derived from a waste biomass as anode material in lithium-ion batteries. *J. Taiwan Inst. Chem. Eng.* **2019**, *95*, 217−226.
(46) Zheng, H.; Feng, C. Q.; Kim, S. J.; Yin, S. Y.; Wu, H. M.; Wang, S. Q.; Li, S. B. Synthesis and electrochemical properties of KMn8O16 nanorods for lithium ion batteries. *Electrochim. Acta* **2013**, *88*, 225−230.
(47) Yang, S. B.; Feng, X. L.; Zhi, L. J.; Cao, Q. A.; Maier, J.; Mullen, K. Nanographene-constructed hollow carbon spheres and their favorable electroactivity with respect to lithium storage. *Adv. Mater.* **2010**, *22*, 838−842.
(48) Jiang, Q.; Zhang, Z.; Yin, S.; Guo, Z.; Wang, S.; Feng, C. Biomass carbon micro/nano-structures derived from ramie fibers and corncobs as anode materials for lithium ion and sodium-ion batteries. *Appl. Surf. Sci.* **2016**, *379*, 73−82.

https://doi.org/10.1021/acsomega.2c03400
ACS Omega 2022, 7, 34109−34116